Stabilization of a Dialkylstannylene by Unusual B−H···Sn γ-Agostic-Type Interactions. A Structural, Spectroscopic, and DFT Study

Keith Izod,* William McFarlane, Brent V. Tyson, Ian Carr, William Clegg, and Ross W. Harrington

Department of Chemistry, School of Natural Sciences, Bedson Building, University of Newcastle, Newcastle upon Tyne, NE1 7RU, U.K.

Received January 3, 2006

The reaction between $SnCl_2$ and the lithium salt $[[\{nPr_2P(BH_3)\}(Me_3Si)CCH_2]Li(THF)_2]_2$ yields the cyclic dialkylstannylene $[\{nPr_2P(BH_3)\}(Me_3Si)CCH_2]_2Sn$ (**6**) as a 1:1 mixture of rac and meso diastereomers. Fractional crystallization from *n*-hexane gives samples of pure *rac*-**6** and *meso*-**6** which have been studied by X-ray crystallography, UV/visible, infrared, and multi-element NMR spectroscopy. In the solid state, *rac*-**6** exhibits two short agostic-type B−H···Sn contacts, one to each BH_3 group, whereas *meso*-**6**, in which both BH_3 groups lie on the same side of the heterocycle, exhibits a single B−H···Sn contact. Multi-element and variable-temperature NMR spectroscopy suggests that these contacts persist in solution, resulting in unusual ^{119}Sn chemical shifts of 587 and 787 ppm for the rac and meso diastereomers, respectively, significantly upfield in comparison to other dialkylstannylenes. Variable-temperature ^{1}H, $^{31}P\{^1H\}$, and $^{11}B\{^1H\}$ NMR studies reveal dynamic equilibria for the meso diastereomer involving competitive binding of the two BH_3 groups to the electron-deficient tin center and restricted rotation about the P−C bond of the free phosphine−borane group. DFT studies confirm that the B−H···Sn contacts are an integral part of the structures; the HOMO and LUMO of both stereoisomers are comprised of an orbital of essentially 5s character on tin and an orbital of predominantly 5p character on tin perpendicular to the plane of the heterocycle, respectively. There is significant donation of electron density from the B−H σ-bonds to the vacant 5p orbital on tin; these B−H···Sn interactions stabilize the electron-deficient Sn(II) center by 30 kcal mol^{-1} for *meso*-**6** and 40 kcal mol^{-1} for *rac*-**6**.

Introduction

There has been significant progress over the past decade in the synthesis of heavier group 14 carbene analogues [tetrylenes, R_2E (E = Si, Ge, Sn, Pb)].[1−11] The vast majority of these compounds are stabilized by the presence of heteroatoms directly adjacent to the heavier tetrel center; of particular note in this regard are the diamidotetrylenes $(R_2N)_2E$ and related compounds, which are analogues of the stable (Arduengo-type) diamidocarbenes.[2−5] In such compounds, the electron-deficient tetrel center is thermodynamically stabilized by a combination

* To whom correspondence should be addressed. E-mail: k.j.izod@ncl.ac.uk.

(1) For recent reviews of heavier tetrylene chemistry, see: (a) Barrau, J.; Rima, G. *Coord Chem. Rev.* **1998**, *178−180*, 593. (b) Tokitoh, N.; Okazaki, R. *Coord. Chem. Rev.* **2000**, *210*, 251. (c) Kira, M. *J. Organomet. Chem.* **2004**, *689*, 4475. (d) Weidenbruch, M. *Eur. J. Inorg. Chem.* **1999**, 373. (e) Klinkhammer, K. W. In *Chemistry of Organic Germanium, Tin and Lead Compounds*; Rappaport, Z., Ed.; Wiley: New York, 2002; Vol. 2, pp 283−357. (f) Veith, M. *Angew. Chem., Int. Ed. Engl.* **1987**, *26*, 1.

(2) For leading references to diamidostannylenes and -plumbylenes, see: (a) Fjeldberg, T.; Hope, H.; Lappert, M. F.; Power, P. P.; Thorne, A. J. *J. Chem. Soc., Chem. Commun.* **1983**, 639. (b) Olmstead, M. M.; Power, P. P. *Inorg. Chem.* **1984**, *23*, 413. (c) Tang, Y.; Felix, A. M.; Zakharov, L. N.; Rheingold, A. L.; Kemp, R. A. *Inorg. Chem.* **2004**, *43*, 7239. (d) Avent, A. G.; Drost, C.; Gehrus, B.; Hitchcock, P. B.; Lappert, M. F. *Z. Anorg. Allg. Chem.* **2004**, *630*, 2090. (e) Gans-Eichler, T.; Gudat, D.; Nieger, M. *Angew. Chem., Int. Ed.* **2002**, *41*, 1888.

(3) For a comprehensive review of the chemistry of *N*-heterocyclic germylenes, see: Kühl, O. *Coord. Chem. Rev.* **2004**, *248*, 411.

(4) For a recent review of *N*-heterocyclic silylenes, see: Hill, N. J.; West, R. *J. Organomet. Chem.* **2004**, *689*, 4165.

(5) For recent reviews of *N*-heterocyclic carbenes, see: (a) Hermann, W. A. *Angew. Chem., Int. Ed.* **2002**, *41*, 1290. (b) Cowley, A. H. *J. Organomet. Chem.* **2001**, *617*, 105. (c) Westkamp, T.; Bohm, V. P. W.; Hermann, W. A. *J. Organomet. Chem.* **2000**, *600*, 12.

(6) (a) Eichler, B. E.; Power, P. P. *Inorg. Chem.* **2000**, *39*, 5444. (b) Phillips, A. D.; Hino, S.; Power, P. P. *J. Am. Chem. Soc.* **2003**, *125*, 7520. (c) Pu, L.; Olmstead, M. M.; Power, P. P.; Schiemenz, B. *Organometallics* **1998**, *17*, 5602. (d) Setaka, W.; Sakamoto, K.; Kira, M.; Power, P. P. *Organometallics* **2001**, *20*, 4460. (e) Eichler, B. E.; Phillips, B. L.; Power, P. P.; Augustine, M. P. *Inorg. Chem.* **2000**, *39*, 5450. (f) Simons, R. S.; Pu, L.; Olmstead, M. M.; Power, P. P. *Organometallics* **1997**, *16*, 1920. (g) Grutzmacher, H.; Pritzkow, H.; Edelmann, F. T. *Organometallics* **1991**, *10*, 23. (h) Wingerter, S.; Gornitzka, H.; Bertermann, R.; Pandey, S. K.; Rocha, J.; Stalke, D. *Organometallics* **2000**, *19*, 3890. (i) Drost, C.; Hitchcock, P. B.; Lappert, M. F.; Pierssens, L. J.-M. *Chem. Commun.* **1997**, 1141. (j) Drost, C.; Hitchcock, P. B.; Lappert, M. F. *Organometallics* **1998**, *17*, 3838. (k) Lay, U.; Pritzkow, H.; Grutzmacher, H. *Chem. Commun.* **1992**, 260. (l) Weidenbruch, M.; Schlaefke, J.; Schafer, A.; Peters, K.; von Schnering, H. G.; Marsmann, H. *Angew. Chem., Int. Ed. Engl.* **1994**, *33*, 1846. (m) Braunschweig, H.; Drost, C.; Hitchcock, P. B.; Lappert, M. F.; Pierssens, L. J.-M. *Angew. Chem., Int. Ed. Engl.* **1997**, *36*, 261. (n) Setaka, W.; Hirai, K.; Sakamoto, K.; Kira, M. *J. Am. Chem. Soc.* **2004**, *126*, 2696. (o) Eichler, B. E.; Pu, L.; Stender, M.; Power, P. P. *Polyhedron* **2001**, *20*, 551. (p) Pu, L.; Phillips, A. D.; Richards, A. F.; Stender, M.; Simons, R. S.; Olmstead, M. M.; Power, P. P. *J. Am. Chem. Soc.* **2003**, *125*, 11626.

(7) (a) Cotton, J. D.; Davidson, P. J.; Lappert, M. F. *J. Chem. Soc., Dalton Trans.* **1976**, 2275. (b) Davidson, P. J.; Harris, D. H.; Lappert, M. F. *J. Chem. Soc., Dalton Trans.* **1977**, 2268. (c) Zilm, K. W.; Lawless, G. A.; Merrill, R. M.; Millar, J. M.; Webb, G. G. *J. Am. Chem. Soc.* **1987**, *109*, 7236.

(8) Kira, M.; Yauchibara, R.; Hirano, R.; Kabuto, C.; Sakurai, H. *J. Am. Chem. Soc.* **1991**, *113*, 7785.

(9) Eaborn, C.; Hill, M. S.; Hitchcock, P. B.; Patel, D.; Smith, J. D.; Zhang, S. *Organometallics* **2000**, *19*, 49.

(10) (a) Engelhardt, L. M.; Jolly, B. S.; Lappert, M. F.; Raston, C. L.; White, A. H. *J. Chem. Soc., Chem. Commun.* **1988**, 336. (b) Jolly, B. S.; Lappert, M. F.; Engelhardt, L. M.; White, A. H.; Raston, C. L *J. Chem. Soc., Dalton Trans.* **1993**, 2653.

10.1021/om0600036 CCC: $33.50
Publication on Web 02/01/2006

Chart 1

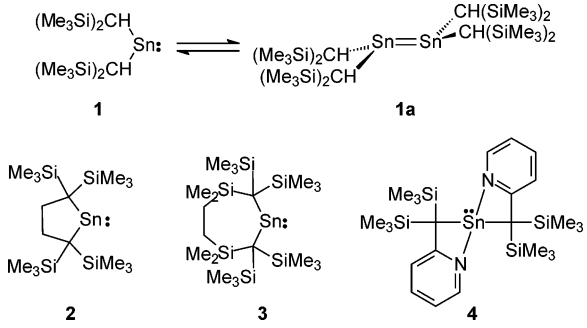

of efficient overlap between the heteroatom lone pairs and the vacant tetrylene p_π orbital and the increased singlet−triplet energy gap, due to stabilization of the sp^2 lone pair on the tetrel atom by the electronegative heteroatom centers.

In comparison to diamidotetrylenes, heavier tetrylenes possessing hydrocarbyl ligands have been less well explored.[1] Thermodynamic stabilization of the tetrylene center is absent in these compounds, which rely solely on kinetic stabilization by sterically demanding substituents. Of the diorganostannylenes reported to date homo- and heteroleptic aryl-substituted stannylenes are the most numerous.[6]

In contrast, dialkylstannylenes are limited to only a very few examples (Chart 1). The archetypal dialkylstannylene $\{(Me_3Si)_2CH\}_2Sn$ (**1**),[7] reported by Lappert and co-workers in 1976, exists as a monomer in the gas phase, but as a dimer [a distannene, $R_2Sn{=}SnR_2$ (**1a**)] in the solid state; in solution, **1** is subject to a monomer−dimer equilibrium (**1** ⇄ **1a**). The first dialkylstannylene shown to exist as a monomer in the solid state, $\{(Me_3Si)_2CCH_2\}_2Sn$ (**2**), was reported by Kira and co-workers in 1991.[8] The "helmet-like" bidentate ligand in this stannylene bears a close resemblance to the two $(Me_3Si)_2CH$ ligands in **1** but provides sufficient steric bulk to disfavor dimerization. Since Kira's original report, only one further dialkylstannylene has been structurally characterized: Eaborn, Smith, and co-workers recently reported the seven-membered cyclic stannylene $\{(Me_3Si)_2C(SiMe_2CH_2)\}_2Sn$ (**3**).[9] In addition, the intramolecularly base-stabilized dialkylstannylene $\{(Me_3Si)_2C(C_5H_4N)\}_2Sn$ (**4**)[10] and a small number of heteroleptic alkylstannylenes of the form RSnX [X = e.g., aryl, halide, etc.] have been isolated,[6f,o,10,11] including a heteroleptic, intramolecularly base-stabilized dialkylstannylene related to **4**.[11a,b]

We have recently become interested in the chemistry of phosphine−borane-stabilized carbanions, $\{R_2P(BH_3)\}CR_2^-$, and noted that $R_2P(BH_3)$ and R_3Si groups are exactly isoelectronic. In the course of our studies into these carbanions, we have synthesized the dicarbanion complex $[\{nPr_2P(BH_3)\}(Me_3Si)CCH_2]Li(THF)_2]_2$ (**5**)[12] and observed its similarity to the silicon-stabilized dicarbanion $[\{(Me_3Si)_2CCH_2\}Li(THF)_2]_2$ originally reported by Eisch and co-workers[13] and subsequently employed by Kira and co-workers in the synthesis of **2**.[8] We thus sought to use our new dicarbanion complex **5** in the synthesis of a novel dialkylstannylene. Herein, we describe the synthesis of this stannylene, its separation into its diastereomers, their solid-state structures, their behavior in solution, their remarkable spectroscopic properties, and details of their unusual electronic structures.

Scheme 1

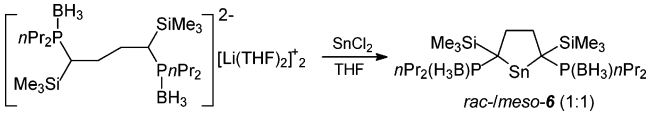

Results and Discussion

Synthesis and Solid-State Structures. The reaction between anhydrous tin(II) chloride and the dilithium salt $[[\{nPr_2P(BH_3)\}(Me_3Si)CCH_2]Li(THF)_2]_2$ (**5**) in THF cleanly gives the dialkylstannylene $[\{nPr_2P(BH_3)\}(Me_3Si)CCH_2]_2Sn$ (**6**) in excellent yield as an air-sensitive yellow solid after a straightforward workup (Scheme 1). Kira and co-workers noted that the closely related compound **2** is isolated only in low yields via this route and that its workup is somewhat difficult;[8] better yields of **2** are obtained by the reduction of the dichlorostannane $\{(Me_3Si)_2CCH_2\}_2SnCl_2$ with KC_8.[14] In contrast, **6** is isolated in excellent yield and purity; we attribute this to an increase in charge delocalization away from the carbanion center in **5** compared to $[\{(Me_3Si)_2CCH_2\}Li(THF)_2]_2$ due to the greater charge delocalizing ability of $R_2P(BH_3)$ in comparison to $SiMe_3$. This makes the former dicarbanion less nucleophilic and, hence, results in a decreased tendency toward reduction of the tin(II) center to elemental tin. However, compound **6** is sensitive to both heat and light, decomposing to give elemental tin and the free phosphine−borane $[\{nPr_2P(BH_3)\}(Me_3Si)CHCH_2]_2$ on exposure to light for extended periods (over 1 week) or when heated to 60°C in hexane solution.

Multi-element [^{1}H, ^{13}C{^{1}H}, ^{11}B{^{1}H}, ^{31}P{^{1}H}, and ^{119}Sn] NMR spectroscopy establishes that **6** is isolated as a 1:1 mixture of the two possible diastereomers under these conditions. Extraction of **6** into *n*-hexane at room temperature yields solutions containing mainly *rac*-**6**; extraction of the residue into warm *n*-hexane gives solutions which contain predominantly *meso*-**6**. Careful crystallization of these fractions from cold *n*-hexane gives samples of pure *rac*- and *meso*-**6** as yellow blocks and yellow needles, respectively, both of suitable quality for X-ray crystallography.

The crystal structures of *rac*- and *meso*-**6** are shown in Figure 1 along with details of selected bond lengths and angles. The two diastereomers crystallize as discrete dialkylstannylene species; the closest Sn···Sn distance in both cases is approximately 7.0 Å. Both *rac*- and *meso*-**6** consist of a five-membered stannacycle with Sn−C distances of 2.2984(14) and 2.3046(14) Å (*rac*-**6**) and 2.272(4) and 2.312(4) Å (*meso*-**6**), respectively. These distances compare with Sn−C distances of 2.218(7) and 2.223(7) Å in the five-membered cyclic stannylene **2**[7] and 2.284(3) and 2.286(3) Å in the seven-membered cyclic stannylene **3**.[9] The C−Sn−C angles are 85.32(5)° and 84.53(15)° in *rac*- and *meso*-**6**, respectively, and these compare with C−Sn−C angles of 86.7(2)° and 117.6(1)° in **2** and **3**,[8,9] respectively; the wide C−Sn−C angle in **3** is a consequence of

(11) (a) Cardin, C. J.; Cardin, D. J.; Constantine, S. P.; Drew, M. G. B.; Rashid, H.; Convery, M. A.; Fenske, D. *J. Chem. Soc., Dalton Trans.* **1998**, 2749. (b) Benet, S.; Cardin, C. J.; Cardin, D. J.; Constantine, S. P.; Heath, P.; Rashid, H.; Teixeira, S.; Thorpe, J. H.; Todd, A. K. *Organometallics* **1999**, *18*, 389. (c) Al-Juaid, S. S.; Avent, A. G.; Eaborn, C.; Hill, M. S.; Hitchcock, P. B.; Patel, D. J.; Smith J. D. *Organometallics* **2001**, *20*, 1223. (d) Leung, W.-P.; Kwok, W.-H.; Zhou, Z.-Y.; Mak, T. C. W. *Organometallics* **2003**, *22*, 1751. (e) Leung, W.-P.; Weng, L.-H.; Kwok, W.-H.; Zhou, Z.-Y.; Zhang, Z.-Y.; Mak, T. C. W. *Organometallics* **1999**, *18*, 1482. (f) Cardin, C. J.; Cardin, D. J.; Constantine, S. P.; Todd, A. K.; Teal, S. J.; Coles, S. *Organometallics* **1998**, *17*, 2144. (g) Eaborn, C.; Hitchcock, P. B.; Smith, J. D.; Sozerli, S. E. *Organometallics* **1997**, *16*, 5653.

(12) Izod, K.; McFarlane, W.; Tyson, B. V.; Clegg, W.; Harrington, R. W. *Chem. Commun*. **2004**, 570.

(13) (a) Eisch, J. J.; Beuhler, R. J. *J. Org. Chem*. **1963**, *28*, 2876. (b) Eisch, J. J.; Gupta, G. *J. Organomet. Chem*. **1973**, *50*, C23.

(14) Kira, M.; Ishida, S.; Iwamoto, T.; Yauchibara, R.; Sakurai, H. *J. Organomet. Chem.* **2001**, *636*, 144.

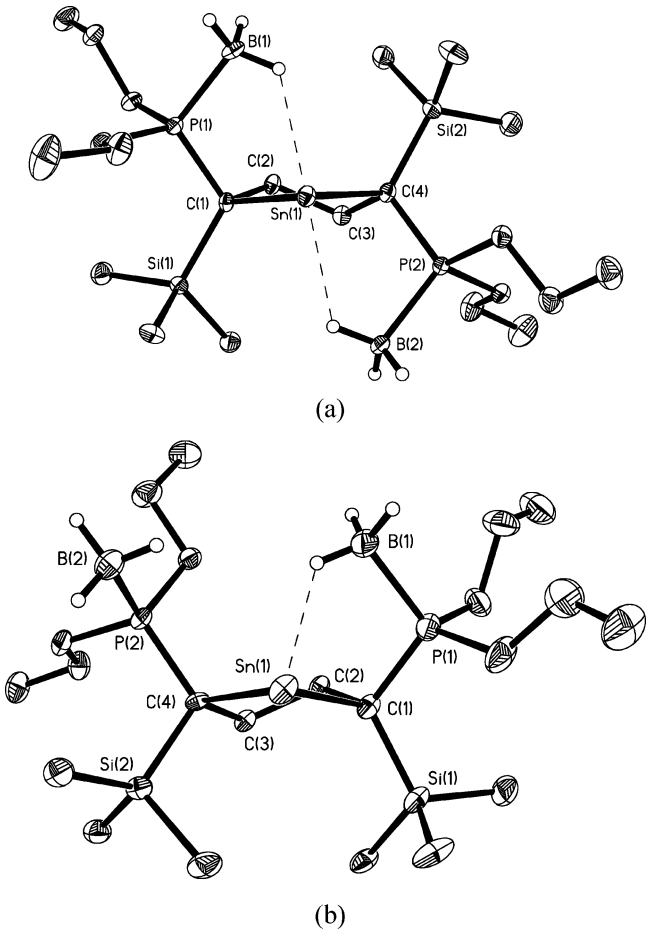

Figure 1. Molecular structures of (a) *rac*-**6** and (b) *meso*-**6** with 40% probability ellipsoids and with H atoms (except those bonded to boron atoms) omitted for clarity. Selected bond lengths (Å) and angles (deg): *rac*-**6**: Sn−C(1) 2.2984(14), Sn−C(4) 2.3046(14), C(1)−P(1) 1.8137(4), C(1)−Si(1) 1.8953(15), C(4)−P(2) 1.8137(14), C(4)−Si(2) 1.8996(15), P(1)−B(1) 1.9317(18), P(2)−B(2) 1.9382(18), Sn···(1C) 2.32(2), Sn···H(1C) 2.32(2), C(1)−Sn−C(4) 85.32(5). *meso*-**6**: Sn−C(1) 2.312(4), Sn−C(4) 2.272(4), C(1)−P(1) 1.802(5), C(1)−Si(1) 1.891(5), C(4)−P(2) 1.817(4), C(4)−Si(2) 1.904(4), P(1)−B(1) 1.933(6), P(2)−B(2) 1.929(6), Sn···H(1B) 2.03(5), C(1)−Sn−C(4) 84.53(15).

the formation of a seven-membered heterocycle and the need to accommodate two tris(trialkylsilyl)methyl groups adjacent to the tin atom.[9] The C−Sn−C angles in *rac*- and *meso*-**6** are somewhat smaller than the corresponding angles in the gas-phase structure of the acyclic dialkylstannylene **1** [96(1)°][7] and the C−Sn−C angles in any of the crystallographically characterized diarylstannylenes, which range from 97° to 115°.[6]

Perhaps the most remarkable features of the structures of *rac*- and *meso*-**6** are the short, agostic-type B−H···Sn contacts; for both *rac*- and *meso*-**6**, the H atoms of the borane groups were located in difference maps and were freely refined. Compound *rac*-**6** has approximate C_2 symmetry, with one borane group situated on either side of the five-membered heterocyclic ring; one hydrogen atom from each borane group lies in close proximity to the electron-deficient Sn(II) center [Sn···H(1C), 2.31(2); Sn···H(2C), 2.37(2) Å]. In *meso*-**6**, both borane groups lie on the same side of the heterocycle and there is only one short Sn···H distance [Sn···H(1B), 2.03(5) Å], although this is significantly shorter than the corresponding distances in *rac*-**6**. These distances are well within the sum of the van der Waals radii of Sn and H (3.37 Å), and the Sn···H distance in *meso*-**6** is just 0.35 Å longer than the sum of the covalent radii of Sn and H (1.68 Å).

To our knowledge, compound **6** represents the first example of a B−H···M agostic-type interaction involving a low-oxidation-state main group metal center. Only one previous example has been reported of a short B−H···Sn contact: the Sn···H distance in the anion of [10-*endo*-($SnPh_3$)-10-μ-*H*-7,8-*nido*-$C_2B_9H_{10}$][*trans*-Ir(CO)(PPh_3)$_2$(MeCN)] (**7**),[15] in which the metal is directly bonded to the boron atom of a carborane cage, is 2.349 Å.

Although such agostic-type P−B−H···M interactions have not previously been observed for main group metals, there have been several recent reports of short contacts between the borane hydrogen atoms of phosphine−borane adducts and transition metal centers. For example, Shimoi and co-workers have isolated complexes of the form M(CO)$_5${H_3BPMe_3} [M = Cr, Mo, W], which are formal analogues of transition metal−alkane σ-complexes;[16] Weller and co-workers have recently reported a range of transition metal complexes of the mixed phosphine/phosphine−borane ligand $Ph_2PCH_2P(BH_3)Ph_2$, which provide models for γ-agostic interactions between transition metals and hydrocarbyl ligands.[17]

The B−H distances for the H atoms associated with the tin centers are similar to the remaining B−H distances in *rac*-**6** [B(1)−H(1C), 1.12(2); B(2)−H(2C), 1.12(2) Å; remaining B−H, 0.99(3)-1.11(2) Å]; in *meso*-**6**, in which there is only one B−H···Sn contact, this B−H distance [B(1)−H(1B), 1.27(5) Å] appears to be somewhat longer than the remaining B−H distances [1.00(7)−1.12(8) Å], although this is still within statistical error. It has been noted that the bridging B−H bonds in M(CO)$_5${H_3BPMe_3} [M = Cr, Mo, W] and related compounds are typically ca. 10% longer than the remaining, terminal B−H bonds.[16,17]

Spectroscopic Characterization. The agostic-type interactions in **6** mitigate the electron deficiency of the Sn(II) centers and have significant consequences for the electronic structure of the molecules and, consequently, for their spectroscopic behavior. The IR spectrum of *rac*-**6** exhibits moderately strong absorptions at 2385, 2174, and 2107 cm^{-1} due to the B−H stretching vibrations; for *meso*-**6**, these vibrations give rise to absorptions at 2439, 2400, 2342, and 2046 cm^{-1}. The absorptions at 2107 and 2046 cm^{-1} for *rac*- and *meso*-**6**, respectively, may be assigned to the B−H···Sn stretching vibrations. DFT calculations (see below) confirm this assignment: frequency calculations indicate that the B−H···Sn stretching vibration(s) lie approximately 270−320 cm^{-1} lower than the terminal B−H stretching vibrations in *rac*-**6** and approximately 260−420 cm^{-1} lower in *meso*-**6**.

Consistent with their pale yellow colors, the UV/visible spectra of *rac*- and *meso*-**6** exhibit absorptions at 338 (ϵ = 3080 $dm^3\ mol^{-1}\ cm^{-1}$) and 360 nm (ϵ = 570 $dm^3\ mol^{-1}\ cm^{-1}$), respectively. This is in marked contrast to the deep red or purple monomeric dialkylstannylenes **2** and **3**,[8,9] which have absorptions at 484 (ϵ = 400 $dm^3\ mol^{-1}\ cm^{-1}$) and 546 nm (ϵ = 175 $dm^3\ mol^{-1}\ cm^{-1}$), respectively; in **2**, this absorption has been

(15) Kim. J.; Kim, S.; Do, Y. *J. Chem. Soc., Chem. Commun.* **1992**, 938.

(16) (a) Shimoi, M.; Nagai. S.-I.; Ichikawa, M.; Kawano, Y.; Katoh, K.; Uruichi, M.; Ogino, H. *J. Am. Chem. Soc.* **1999**, *121*, 11704. (b) Kakizawa, T.; Kawano, Y.; Shimoi, M. *Organometallics* **2001**, *20*, 3211. (c) Shimoi, M.; KAtoh, K.; Kawano, Y.; Kodama, G.; Ogino, H. *J. Organomet. Chem.* **2002**, *659*, 102.

(17) (a) Ingleson, M.; Patmore, N. J.; Ruggiero, G. D.; Frost, C. G.; Mahon, M. F.; Willis, M. C.; Weller, A. S. *Organometallics* **2001**, *20*, 4434. (b) Merle, M.; Koicok-Kohn, G, Mahon, M. F.; Frost, C. G.; Ruggiero, G. D.; Weller, A. S.; Willis, M. C. *Dalton Trans.* **2004**, 3883.

attributed to the transition between the lone pair and the vacant 5p orbital on tin. Clearly, the observed B−H···Sn interactions cause a significant perturbation of these orbitals and a consequent shift in this absorption; for comparison, the compound $\{2,4,6\text{-}(CF_3)_3C_6H_2\}_2Sn$ (**7**),[6g] in which the electron deficiency of the Sn(II) center is mitigated by short C−F···Sn contacts, has $\lambda_{max} = 345$ nm ($\epsilon = 1534$ dm^3 mol^{-1} cm^{-1}).

Multi-element and variable-temperature NMR spectroscopy also indicate that the agostic-type B−H···Sn interactions observed in the solid-state persist in solution. At room temperature, the ^{1}H NMR spectra of *rac*- and *meso*-**6** are as expected, although in the latter compound, only a single resonance is observed for the BH_3 and $SiMe_3$ groups, suggesting that *meso*-**6** is subject to a dynamic process in solution by which the two distinct environments observed for each of these groups in the solid state are averaged on the NMR time scale (see below). The $SiMe_3$ groups give rise to sharp singlets at 0.25 and 0.14 ppm in the ^{1}H NMR spectra of *rac*- and *meso*-**6**, respectively. The BH_3 resonances of both *rac*- and *meso*-**6** are so broad that they are virtually indistinguishable from the baseline; these signals collapse on decoupling the quadrupolar ^{11}B nuclei to give broad doublets at approximately 0.90 and 1.07 ppm for *rac*- and *meso*-**6**, respectively ($^2J_{PH} = 7.6$ Hz in both cases). The propyl substituents give rise to a sequence of complex multiplets between 0.77 and 2.03 ppm (*rac*-**6**) and between 0.84 and 1.88 ppm (*meso*-**6**), whereas the backbone CH_2CH_2 protons give rise to complex multiplets at 2.30 and 2.87 ppm (*rac*-**6**) and 2.36 and 2.69 ppm (*meso*-**6**). The ^{13}C{^{1}H} spectra of *rac*- and *meso*-**6** are essentially as expected: the quaternary carbon centers give rise to broad signals at 38.14 and 42.00 ppm, respectively; satellites due to coupling to the tin nuclei were not resolved in either case.

The ^{31}P{^{1}H} spectra consist of broad, poorly resolved quartets centered at 22.3 and 23.4 ppm for the *rac*- and *meso*-diastereomers, respectively [$^1J_{PB} = 82$ Hz, $\Delta\nu_{1/2} = 240$ Hz (*rac*-**6**); $^1J_{PB} = 93$ Hz, $\Delta\nu_{1/2} = 240$ Hz (*meso*-**6**)], and the ^{11}B{^{1}H} spectra consist of broad doublets at −34.5 [$\Delta\nu_{1/2} = 180$ Hz] and −33.2 ppm [$\Delta\nu_{1/2} = 180$ Hz], respectively.

One of the most significant effects of the agostic-type B−H···Sn interactions in *rac*- and *meso*-**6** is observed in their ^{119}Sn spectra: *rac*- and *meso*-**6** give rise to very broad, featureless resonances at 587 and 787 ppm, respectively, in which coupling to ^{11}B and ^{31}P is not resolved [$\Delta\nu_{1/2} = 430$ and 330 Hz, respectively]. These chemical shifts compare with a shift of 2323 ppm for the structurally analogous five-membered cyclic dialkylstannylene **2**,[8] a difference of more than 1500 ppm; the closely related acyclic dialkylstannylene **1** and the seven-membered cyclic stannylene **3** have ^{119}Sn chemical shifts of 2315 and 2299 ppm, respectively.[7,9] Since **6** and **2** differ only in the substitution of two $R_2P(BH_3)$ groups for two exactly isoelectronic $SiMe_3$ groups, this difference in chemical shift may be attributed to the difference in electron density at the Sn(II) centers caused by the agostic-type B−H···Sn interactions. The lower chemical shift of *rac*-**6**, in which there are two agostic-type B−H···Sn contacts, compared to *meso*-**6**, in which there is only one, appears to further corroborate this premise. While the ^{119}Sn chemical shifts of **6** are substantially lower than those of closely related dialkylstannylenes, they are similar to those of the diarylstannylenes $\{2,6\text{-}(2,4,6\text{-}Me_3C_6H_2)_2C_6H_3\}_2Sn$ (635 ppm)[6f] and **7** (723 ppm).[6g]

The extremely broad nature of the ^{119}Sn signals and the lack of observable tin satellites in the ^{13}C{^{1}H} and ^{31}P{^{1}H} spectra of *rac*- and *meso*-**6** are consistent with the presence of a low-concentration, possibly tin-centered, radical, most likely arising from thermal or photolytic decomposition of the samples, which is in rapid exchange with diamagnetic **6**. Unfortunately, attempts to detect such a radical species by EPR spectroscopy were unsuccessful.

The ^{1}H, ^{11}B{^{1}H}, and ^{31}P{^{1}H} spectra of *rac*-**6** in d_8-toluene are invariant over the temperature range 303−183 K. In contrast, the corresponding spectra of *meso*-**6** reveal that this compound is subject to dynamic processes in solution. As the temperature is reduced below ambient, the signals in the ^{1}H{^{11}B} NMR spectrum in the region associated with the propyl groups and the CH_2CH_2 backbone protons become significantly broader and more complex and increasingly difficult to interpret. However, the signal due to the $SiMe_3$ groups broadens as the temperature is reduced until, at approximately 208 K, it decoalesces into two very broad, equal-intensity signals at 0.00 and 0.31 ppm; these signals sharpen as the temperature is reduced further, and at 188 K, two relatively sharp singlets are observed. The BH_3 resonances broaden and become obscured by the propyl resonances as the temperature decreases; this is partly a consequence of increased broadening by the ^{11}B nuclei at lower temperatures and to difficulties in effectively decoupling the ^{1}H and ^{11}B nuclei.

A clearer picture of the solution behavior of *meso*-**6** is provided by its variable-temperature ^{31}P{^{1}H} and ^{11}B{^{1}H} spectra. The ^{31}P{^{1}H} spectrum of *meso*-**6** at 291 K consists of a poorly resolved, broad quartet (Figure 2a). This signal broadens as the temperature is lowered and decoalesces below 232 K into two signals at 18.3 and 25.1 ppm, the higher-field signal of which is considerably sharper than the lower-field signal. As the temperature is decreased, these signals broaden and decoalesce further until, at 183 K, the spectrum consists of two large, equal-intensity, poorly resolved quartets at 16.7 (**A**) and 22.2 ppm (**B**) along with two smaller signals (∼16% intensity of the major signals), one (**C**) partially obscured by signal **A**, at approximately 18 ppm, and the other (**D**) at 34.0 ppm. The variable-temperature ^{11}B{^{1}H} spectra of *meso*-**6** also exhibit significant broadening at lower temperatures (Figure 3). Below 213 K, the broad doublet observed at room temperature decoalesces into two very broad signals of approximately equal intensity. As the temperature decreases, these signals decoalesce further until, at 183 K, the spectrum consists of two very broad signals at −31 (**E**) and −34 ppm (**F**), the high-field signal of which partially obscures a new moderate-intensity signal at approximately −36 ppm (**G**).

These spectra are consistent with the operation of two distinct dynamic equilibria in solution. We attribute the higher-energy process to competitive binding of the two BH_3 groups to the Sn(II) center (Scheme 2), which is rapid on the NMR time scale at room temperature but which may be frozen out below 232 K. Thus, at low temperatures, the solution-state structure resembles that observed in the solid state, and so there are two distinct $SiMe_3$ and $PPr_2(BH_3)$ environments.

Below 213 K, the operation of a second dynamic process becomes apparent. We initially considered that this might be due to a monomer−dimer (i.e., stannylene−distannene) equilibrium, related to that observed for the stannylene **1** in solution. Unfortunately, for *meso*-**6**, a variable-temperature ^{119}Sn NMR experiment was uninformative in this regard: the ^{119}Sn signal broadens significantly as the temperature is reduced until, below 213 K, the signal is indistinguishable from the baseline; *rac*-**6** exhibits similar behavior. In contrast, the ^{119}Sn spectrum of **1** at 165 K exhibits signals at 2315 ppm and at 740 and 725 ppm due to the stannylene and distannene forms, respectively.[7]

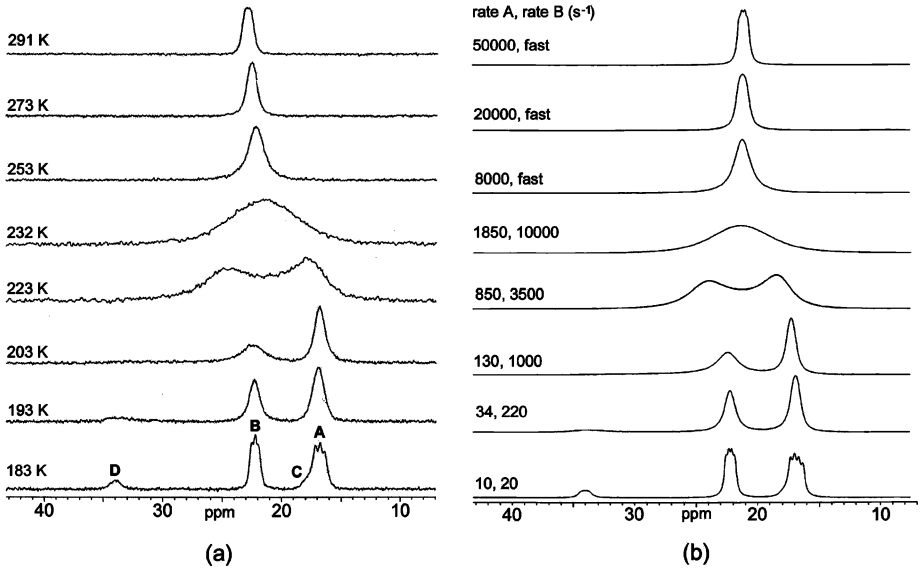

Figure 2. (a) Observed and (b) simulated variable-temperature $^{31}P\{^1H\}$ NMR spectra of *meso*-**6** in d_8-toluene. Rate A, exchange between the free and bound $PPr_2(BH_3)$ groups; rate B, exchange between rotamers of the free $PPr_2(BH_3)$ group.

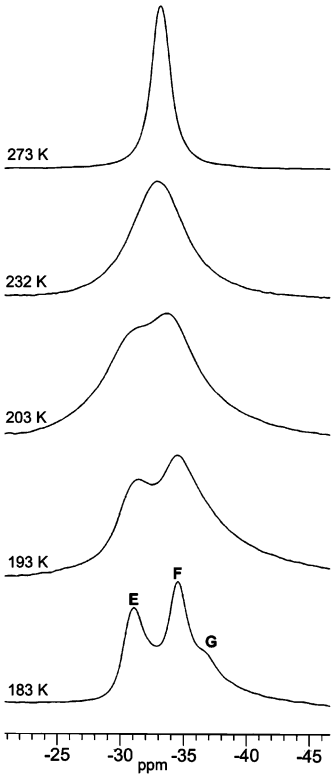

Figure 3. Variable-temperature $^{11}B\{^1H\}$ NMR spectra of *meso*-**6** in d_8-toluene.

Scheme 2

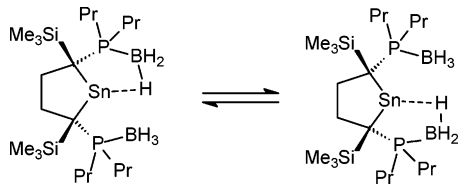

A stannylene−distannene equilibrium for *meso*-**6** should generate two distinct distannene isomers (Scheme 3a) and so should result in a much more complex ^{31}P spectrum at low temperatures than is observed. Although it is possible that only the symmetric isomer of the distannene is accessible, variable-concentration experiments suggest that formation of distannene species at low temperature is unlikely under the conditions used: $^{31}P\{^1H\}$ spectra of samples of *meso*-**6** at concentrations of 0.25 and 0.05 M recorded at temperatures between 273 and 188 K are essentially indistinguishable. Simulation of the variable-temperature $^{31}P\{^1H\}$ spectra of *meso*-**6** (Figure 2(b)) and a subsequent line shape analysis yields values of $\Delta H^{\ddagger} = 34 \pm 1$ kJ mol^{-1} and $\Delta S^{\ddagger} = -35 \pm 4$ J K^{-1} mol^{-1} for the phosphine−borane exchange process, and $\Delta H^{\ddagger} = 41 \pm 2$ kJ mol^{-1} and $\Delta S^{\ddagger} = 10 \pm 10$ J K^{-1} mol^{-1} for the dynamic process observed at lower temperatures; this is consistent with an intramolecular process in both cases. We note that the closely related cyclic stannylene **2** is monomeric in both the solid state and in solution and that *rac*-**6** does not exhibit dynamic behavior in its NMR spectra. We note also that poorly resolved splitting by ^{11}B is apparent in the ^{31}P spectrum of *meso*-**6** at 291 K, thus confirming, as expected, that this dynamic process does not involve P−B bond cleavage.

Scheme 3[a]

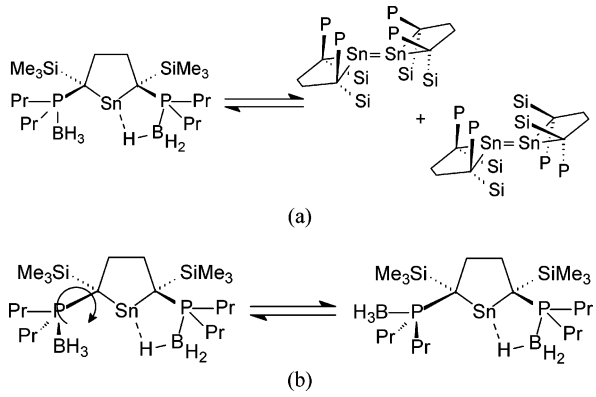

[a] Si = $SiMe_3$, P = $P(BH_3)nPr_2$

We therefore propose that the dynamic process observed below 213 K is associated with a restricted rotation about the highly sterically hindered P−C bond of the free phosphine-borane group (Scheme 3b). The low-temperature NMR spectra are thus consistent with the presence of two rotamers, one of which is significantly favored over the other; Newman projections of the three principal rotamers of *meso*-**6** are illustrated in Chart 2. It is to be expected that the two observed dynamic

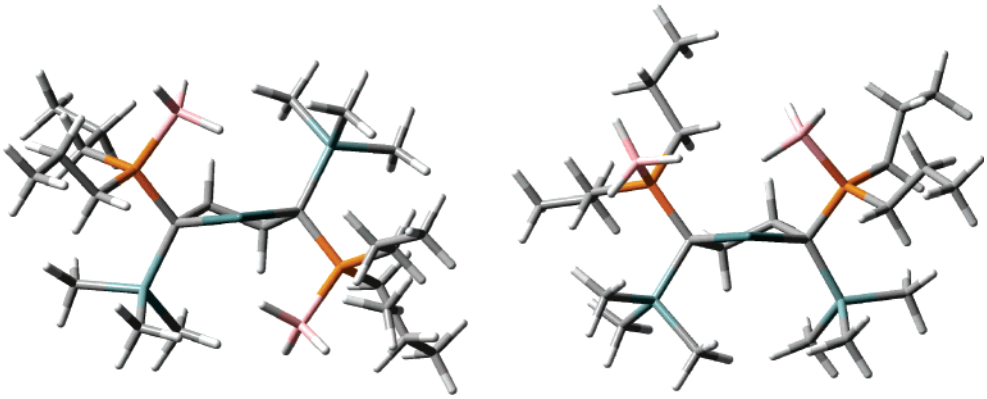

Figure 4. Calculated structures for (a) *rac*-**6a** and (b) *meso*-**6a**.

Chart 2. Newman Projections of the Three Principal Rotamers of *meso*-6 Viewed along the P−C Bond of the Free Phosphine−Borane Group

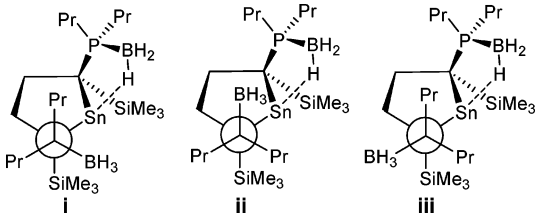

processes (exchange of coordinated and free phosphine−borane groups and rotation about the P−C bond of the free phosphine-borane group) will be somewhat interdependent and thus that the ability of a particular rotamer to participate in the phosphine−borane exchange process will influence its abundance. In rotamers **i** and **ii**, the BH_3 groups are positioned such that they are able to participate readily in the process involving exchange of the free and bound BH_3 groups. The ease of this exchange will probably be different in rotamers **i** and **ii**, so that they will have different energies and therefore different abundances; for rotamer **iii**, the borane exchange process would be disfavored. Thus, rotamers **i** and **ii** have a significant abundance, whereas rotamer **iii** is not observed. On purely steric grounds, rotamers **i** and **ii** are likely to be more stable than rotamer **iii** since in the latter rotamer the two propyl groups lie close to the bulky $SiMe_3$ group and the sterically occluded tin center.

Restricted rotation about the P−C bond can be expected to affect the chemical shift of the free phosphine−borane group more than that of the bound group, and so we tentatively assign the low-field signals **B** and **D** in the low-temperature $^{31}P\{^1H\}$ NMR spectra to the free phosphine−borane group and the high-field signals **A** and **C** to the phosphine−borane group associated with the B−H···Sn agostic-type interaction.

Unfortunately, we were unable to distinguish the unique B−H···Sn proton signals from the remaining B−H resonances in the low-temperature ^1H or $^1H\{^{11}B\}$ spectra of either *rac*- or *meso*-**6** over the temperature range available to us, and so we were unable to observe directly the B−H···Sn contact by this means. However, it is likely that exchange between individual hydrogen atoms within a single BH_3 group is a very low-energy process and that this will be extremely fast on the NMR time scale. Shimoi and co-workers have estimated that the free energy of activation $\Delta G^{\ddagger}$ for exchange between the terminal and bridging H atoms in $M(CO)_5\{\eta^1\text{-}H_3BPMe_3\}$ [M = Cr, Mo, W] is less than 30 kJ mol^{-1} at 193 K.[16]

DFT Calculations. To gain further insight into the nature of the Sn···H interactions in these molecules, we have undertaken a DFT study of both diastereomers. So that all steric and electronic effects were taken into consideration, we have modeled the geometries of the complete molecules; while this is computationally expensive, it allows an exact comparison between the solid-state structures determined by X-ray crystallography and the calculated gas-phase structures of *rac*- and *meso*-**6**. Geometries were optimized using the B3LYP hybrid functional[18] with an effective core potential Lanl2dz basis set[19] on the tin atoms and an all-electron 6-31G(d,p) basis set on the remaining atoms.[20]

Table 1. Comparison of Selected Bond Lengths (Å) and Angles (deg) for *rac*-6 and 6a and for *meso*-6 and 6a

	rac-**6**	*rac*-**6a**	*meso*-**6**	*meso*-**6a**
Sn−C(1)	2.2984(14)	2.324	2.312(4)	2.370
Sn−C(4)	2.3046(14)	2.342	2.272(4)	2.301
Sn···H(1X)	2.31(2)	2.341	2.03(5)	2.155
Sn···H(2X)	2.37(2)	2.348		
C(1)−P(1)	1.8137(14)	1.847	1.802(5)	1.836
C(1)−Si(1)	1.8953(15)	1.928	1.891(5)	1.921
C(4)−P(2)	1.8137(14)	1.843	1.817(4)	1.854
C(4)−Si(2)	1.8996(15)	1.929	1.904(4)	1.939
B(1)−H(1X)[a]	1.12(2)	1.240	1.27(5)	1.255
B(2)−H(2)	1.12(2)	1.240		
C(1)−Sn−C(4)	85.32(5)	85.25	84.53(15)	83.99

[a] X = C (*rac*-**6**), B (*meso*-**6**).

The calculated structures of the two diastereomers (*rac*-**6a** and *meso*-**6a**, respectively) are remarkably similar to those determined crystallographically; the structures of *rac*- and *meso*-**6a** are shown in Figure 4, and a comparison of selected bond lengths and angles for both stereoisomers of **6** and **6a** is given in Table 1. In general, bond lengths in the calculated structures are slightly longer, by approximately 0.03−0.07 Å, than those determined crystallographically; for example, the Sn−C distances in *rac*-**6** are 2.3046(14) and 2.2984(14) Å and in *rac*-**6a** these are 2.342 and 2.324 Å, while the Sn−C distances in *meso*-**6** are 2.272(4) and 2.312(4) Å and in *meso*-**6a** these are 2.301 and 2.370 Å. However, the calculated angles are very close to those observed in the solid state; the C−Sn−C angles for *rac*-**6** and *rac*-**6a** are 85.32(5)° and 85.25°, respectively, whereas the corresponding angles for *meso*-**6** and *meso*-**6a** are 84.53(15)° and 83.99°, respectively.

The calculated gas-phase structures of *rac*- and *meso*-**6a** replicate the close H···Sn contacts observed in the solid state

(18) (a) Becke A. D. *J. Chem. Phys.* **1993**, *98*, 5648. (b) Stephens, P. J.; Devlin, F. J.; Chablowski, C. F.; Frisch, M. J. *J. Phys. Chem.* **1994**, *98*, 11623. (c) Hertwig, R. H.; Koch, W. *Chem. Phys. Lett.* **1997**, *268*, 345.

(19) (a) Hay, P. J.; Wadt, W. R. *J. Chem. Phys.* **1985**, *82*, 270. (b) Wadt, W. R.; Hay, P. J. *J. Chem. Phys.* **1985**, *82*, 284. (c) Hay P. J.; Wadt, W. R. *J. Chem. Phys.* **1985**, *82*, 299.

(20) (a) Hariharan, P. C.; Pople, J. A. *Theor. Chim. Acta* **1973**, *28*, 213. (b) Francl, M. M.; Petro, W. J.; Hehre, W. J.; Binkley, J. S.; Gordon, M. S.; DeFrees, D. J.; Pople, J. A. *J. Chem. Phys.* **1982**, *77*, 3654.

for *rac*- and *meso*-**6** extremely well: there are two short Sn···H contacts in *rac*-**6a**, in which the two borane groups are on either side of the heterocycle, and one short Sn···H contact in *meso*-**6a**, in which both borane groups are on the same side of the heterocycle. The Sn···H distances in *rac*-**6a** are 2.34 and 2.35 Å, while the Sn···H distance in *meso*-**6a** is 2.14 Å; these compare with Sn···H distances of 2.31(2) and 2.37(2) Å in *rac*-**6** and 2.03(5) Å in *meso*-**6**. Clearly, the shorter Sn···H distances, and thus the stronger interactions, in *meso*-**6**/**6a** appear to be a direct consequence of the availability of only one borane group with which to form an agostic-type interaction in this diastereomer; in *rac*-**6**/**6a** the electron deficiency of the Sn(II) center is mitigated by the formation of two weaker, agostic-type interactions (see below).

The B−H bonds associated with the B−H···Sn contact in both *rac*-**6a** and *meso*-**6a** are slightly elongated (1.24/1.24 and 1.26 Å, respectively) in comparison to the remaining B−H bonds, which span the range 1.20−1.22 Å. In accord with an agostic-type interaction, population analysis reveals an accumulation of charge at the hydrogen atoms associated with these interactions. Thus, in *rac*-**6a**, these hydrogen atoms have Mulliken charges of −0.18 (for each of the two hydrogen atoms close to the tin center) compared to charges ranging from −0.08 to −0.09 on the remaining borane H atoms; in *meso*-**6a**, the charge on the H atom associated with the tin center is calculated to be −0.19 compared with charges ranging from −0.07 to −0.10 on the remaining borane H atoms. For comparison, Durig and Shen have calculated that the borane hydrogen atoms in the neutral adduct H_3BPH_3 have a Mulliken charge of −0.01 but that this increases to −0.035 in H_3BPF_3.[21]

Consistent with the increased stabilization by two agostic-type B−H···Sn interactions in *rac*-**6a** compared to one such interaction in *meso*-**6a**, the calculated energy of *rac*-**6a** is lower than that of the meso diastereomer, although by just 5.7 kcal mol^{-1}.

The nature of the HOMO and LUMO and of the interaction between the tin centers and the borane groups in both *rac*- and *meso*-**6a** was probed via natural bond orbital (NBO) analyses;[22] the HOMO and LUMO of *rac*- and *meso*-**6a** are illustrated in Figure 5. The calculated HOMO in both cases is largely comprised of a lone pair on tin of essentially 5s character, whereas the LUMO in each case is comprised predominantly of the vacant $5p_x$ orbital on tin which lies perpendicular to the plane of the heterocycle. There are significant interactions between the vacant Sn $5p_x$ orbitals and the B−H σ-orbitals in both diastereomers. The NBO analyses reveal that there is substantial delocalization of the B−H σ-bonding electron density into the Sn $5p_x$ orbital, from two B−H bonds in *rac*-**6a** and one B−H bond in *meso*-**6a**. Analysis of the donor−acceptor interactions reveals that these agostic-type interactions stabilize *rac*- and *meso*-**6a** by 40 (i.e., 2 × 20) and 30 kcal mol^{-1}, respectively.

Conclusions

The novel diastereomeric dialkylstannylene **6** may be synthesized in excellent yield and readily separated into its constituent diastereomers. The electron deficiency at the Sn(II) centers in **6** is mitigated by unique, agostic-type B−H···Sn interactions: one such interaction in the case of *meso*-**6** and two in the case of *rac*-**6**. Spectroscopic studies clearly indicate that the short B−H···Sn contacts observed by X-ray crystallography persist in solution; these contacts have a marked effect on the ^{119}Sn chemical shifts of *rac*- and *meso*-**6**, which are more than 1500 ppm lower than the chemical shift observed for the corresponding silicon-substituted stannylene **2**. Variable-temperature NMR spectroscopy suggests that *meso*-**6** is subject to two independent dynamic equilibria involving (i) exchange between the coordinated and free BH_3 groups and (ii) restricted rotation about the P−C bond of the free phosphine-borane group. DFT calculations indicate that the B−H···Sn agostic-type interactions stabilize *rac*- and *meso*-**6** by ca. 40 and 30 kcal mol^{-1}, respectively, via substantial donation of the B−H bonding electron density into the vacant 5p orbital on tin (the LUMO in each case).

Thus, the incorporation of phosphine−borane functionality provides a novel method for the stabilization of electron-deficient dialkyltetrylenes. We are currently investigating whether agostic-type B−H···Sn and related interactions may be used to provide sufficient stabilization to enable the isolation of less sterically hindered diorganotetrylenes than **6**.

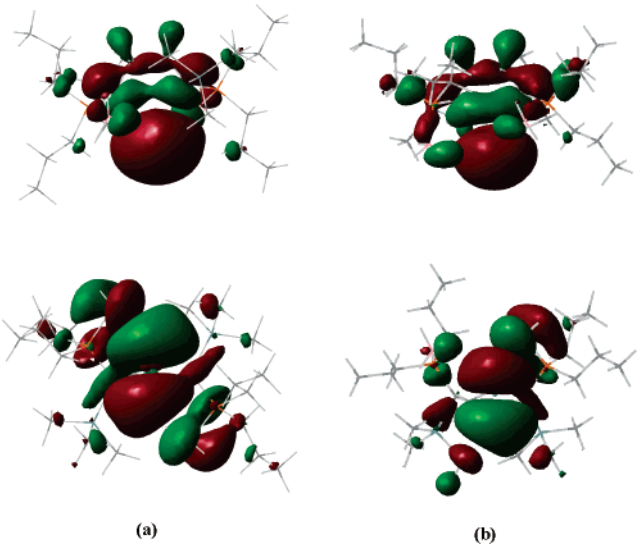

Figure 5. HOMO (upper) and LUMO (lower) of (a) *rac*-**6a** and (b) *meso*-**6a**.

Experimental Section

All manipulations were carried out using standard Schlenk techniques under an atmosphere of dry nitrogen or argon. Ether, *n*-hexane, and light petroleum (bp = 40−60 °C) were distilled under nitrogen from sodium/potassium alloy; all solvents were stored over a potassium film. Deuterated toluene was distilled from potassium and deoxygenated by three freeze−pump−thaw cycles and was stored over activated 4 Å molecular sieves. All compounds were used as supplied by the manufacturer except $[\{^n Pr_2P(BH_3)\}(Me_3Si)CCH_2]Li(THF)_2]_2$ (**5**),[12] which was prepared by a previously published method.

NMR spectra were recorded on a JEOL Lambda500 spectrometer operating at 500.16 (^{1}H), 125.65 (^{13}C), 160.35 (^{11}B), 99.25 (^{29}Si), 202.47 (^{31}P), and 186.50 (^{119}Sn) MHz; chemical shifts are quoted in ppm relative to tetramethylsilane (^{1}H, ^{13}C, and ^{29}Si), external $BF_3(OEt_2)$ (^{11}B), external 85% H_3PO_4 (^{31}P), and external Me_4Sn (^{119}Sn), as appropriate. The positions of the BH_3 signals in the ^{1}H NMR spectra of *rac*- and *meso*-**6** and J_{PH} for these signals were

(21) Durig, J. R.; Shen, Z. *J. Mol. Struct. (THEOCHEM)* **1997**, *397*, 179.

(22) (a) Carpenter, J. E.; Weinhold, F. *J. Mol. Struct. (THEOCHEM)* **1988**, *169*, 41. (b) Carpenter, J. E. PhD thesis, University of Wisconsin, Madison, WI, 1987. (c) Foster, J. P.; Weinhold, F. *J. Am. Chem. Soc.* **1980**, *102*, 7211. (d) Reed, A. E.; Weinhold, F. *J. Chem. Phys.* **1983**, *78*, 4066. (e) Reed, A. E.; Weinhold, F. *J. Chem. Phys.* **1983**, 1736. (f) Reed, A. E.; Weinstock, R. B.; Weinhold, F. *J. Chem. Phys.* **1985**, *83*, 735. (g) Reed, A. E.; Curtiss, L. A.; Weinhold, F. *Chem. Rev.* **1988**, *88*, 899.

determined using a selective $^1H\{^{11}B\}$ experiment. X-band EPR spectra were recorded at 295 and 77 K as solutions/frozen solutions in toluene on a Bruker EMX spectrometer. UV/vis spectra were recorded in matched quartz cells as 1.0 mM solutions in methylcyclohexane on a Hitachi U-3010 spectrometer; infrared spectra were recorded as powders on a Nicolet Avatar 370DTGS spectrometer. Elemental analyses were obtained by the Elemental Analysis Service of London Metropolitan University.

Preparation of [{*n*$Pr_2P(BH_3)$}$(Me_3Si)CCH_2]_2Sn$ (6). To a cold (−78 °C) slurry of $SnCl_2$ (0.52 g, 2.74 mmol) in diethyl ether (20 mL) was added, dropwise, a solution of [{*n*$Pr_2P(BH_3)$}(Me_3Si)-$CCH_2]_2Li_2(THF)_4$ (1.85 g, 2.42 mmol) in diethyl ether (30 mL), excluding light as much as possible. This mixture was allowed to attain room temperature and was stirred for 18 h. Solvent was removed in vacuo, and the sticky solid was extracted into warm *n*-hexane (50 mL) and filtered. The solution was concentrated to ca. 10 mL and was cooled to −30 °C for 24 h. The yellow crystals of *rac*-/*meso*-**6** (1:1) were isolated by filtration and were washed with a little cold (−78 °C) light petroleum. Yield 1.43 g, 78%. Anal. Calcd for $C_{22}H_{56}P_2Si_2B_2Sn$: C, 45.87; H, 9.27%. Found: C, 45.63; H, 9.75%.

The rac and meso isomers of **6** were separated by the following procedure. The 1:1 mixture of crystalline *rac*- and *meso*-**6** was extracted into *n*-hexane (10 mL) at room temperature, leaving a yellow residue, and this extract was cooled to 5 °C for 18 h to give a crop of predominantly cube-shaped crystals of *rac*-**6**. The mother liquor was warmed slightly until the small amount of needle-shaped crystals of *meso*-**6** had dissolved, and the crystals of pure *rac*-**6** were isolated by filtration. The yellow residue from the initial extraction was extracted into hot (50 °C) *n*-hexane, and the yellow solution was filtered, concentrated to 5 mL, and cooled to 5 °C for 18 h. The pale yellow, needle-shaped crystals of *meso*-**6** were isolated by filtration and washed with a little cold (−78 °C) light petroleum.

Spectroscopic data for *rac*-**6**: ^1H NMR (d_8-toluene, 20 °C): δ 0.25 (s, 18H, $SiMe_3$), 0.77 (t, 6H, $CH_2CH_2CH_3$), 0.83 (t, 6H, CH_2-CH_2CH_3), 0.90 (br d, J_{PH} = 7.6 Hz, 6H, BH_3), 1.31−2.03 (m, 16H, $CH_2CH_2CH_3$), 2.30 (m, 2H, CH_2CH_2), 2.87 (m, 2H, CH_2CH_2). $^{13}C\{^1H\}$NMR (d_8-toluene, 20 °C): δ 3.11(d, J_{PC} = 2.0 Hz, $SiMe_3$), 16.21 (d, J_{PC} = 6.4 Hz, CH_2CH_3), 16.32 (d, J_{PC} = 6.2 Hz, CH_2CH_3), 17.62 (CH_2CH_3), 18.73 (CH_2CH_3), 31.01 (d, J_{PC} = 10.2 Hz, CH_2P), 31.25 (d, J_{PC} = 3.2 Hz, CH_2P), 38.14 (d, J_{PC} = 5.3 Hz, CSn), 39.73 (d, J_{PC} = 15.6 Hz, CH_2CH_2). $^{11}B\{^1H\}$ NMR (d_8-toluene, 20 °C): δ −34.5 (br d, J_{PB} = 82 Hz). $^{29}Si\{^1H\}$ NMR (d_8-toluene, 20 °C): δ = 2.57 (d, J_{PSi} = 9.1 Hz). $^{31}P\{^1H\}$ NMR (d_8-toluene, 20 °C): δ 22.3 (br q, J_{PB} = 82 Hz). ^{119}Sn NMR (d_8-toluene, 20 °C) δ 578 (br). UV/vis: λ_{max} 338 nm (ϵ = 3080 $dm^3\ mol^{-1}\ cm^{-1}$). IR: 2963 (m), 2931 (m), 2872 (m), 2832 (m), 2817 (m), 2385 (m), 2174 (w), 2107 (m), 1455 (m), 1405 (w), 1738 (w), 1247 (s), 1078 (s), 1050 (m), 1029 (m), 976 (w), 900 (s), 833 (s), 757 (s), 686 (m), 675 (m), 646 (s), 594 (s), 459 (s), 444 (s), 416 (m) cm^{-1}.

Spectroscopic data for *meso*-**6**: ^1H NMR (d_8-toluene, 20 °C): δ 0.14 (s, 18H, $SiMe_3$), 0.84 (m, 12H, $CH_2CH_2CH_3$), 1.07 (br d, J_{PH} = 7.6 Hz, 6H, BH_3), 1.16−1.88 (m, 16H, $CH_2CH_2CH_3$), 2.36 (m, 2H, CH_2CH_2), 2.69 (m, 2H, CH_2CH_2). $^{13}C\{^1H\}$NMR (d_8-toluene, 20 °C): δ 2.35 (d, J_{PC} = 2.1 Hz, $SiMe_3$), 16.26 (d, J_{PC} = 13.8 Hz, CH_2CH_3), 16.38 (d, J_{PC} = 13.6 Hz, CH_2CH_3), 17.57 (CH_2-CH_3), 18.45 (CH_2CH_3), 29.81 (d, J_{PC} = 26.5 Hz, CH_2P), 31.25 (d, J_{PC} = 33.4 Hz, CH_2P), 39.86 (CH_2CH_2), 42.00 (CSn). $^{11}B\{^1H\}$ NMR (d_8-toluene, 20 °C): δ −33.2 (br, d, J_{PB} = 93 Hz). $^{29}Si\{^1H\}$ NMR (d_8-toluene, 20°C): δ = 0.98 (d, J_{PSi} = 3.7 Hz). $^{31}P\{^1H\}$ NMR (d_8-toluene, 20 °C): δ 23.4 (br, d, J_{PB} = 93 Hz). ^{119}Sn NMR (d_8-toluene, 20°C): δ 787 (br). UV/vis: λ_{max} 360 nm (ϵ = 570 $dm^3\ mol^{-1}\ cm^{-1}$). IR: 2962 (m), 2930 (m), 2871 (m), 2439 (w), 2400 (m), 2342 (m), 2046 (m), 1456 (w), 1405 (w), 1380 (w), 1261 (m), 1248 (s), 1218 (w), 1081 (m), 1067 (s), 1040 (m), 979 (m), 904 (s), 852 (s), 826 (s), 779 (m), 752 (m), 734 (m), 679 (m), 640 (s), 623 (m), 590 (s), 463 (m), 434 (m) cm^{-1}.

Table 2. Crystallographic Data for *rac*-6 and *meso*-6[a]

	rac-**6**	*meso*-**6**
formula	$C_{22}H_{56}B_2P_2Si_2Sn$	$C_{22}H_{56}B_2P_2Si_2Sn$
fw	579.1	579.1
cryst size, mm	0.15 × 0.15 × 0.15	0.20 × 0.10 × 0.10
cryst syst	monoclinic	monoclinic
space group	$P2_1/n$	$P2_1/n$
a, Å	11.3845(8)	7.0626(4)
b, Å	17.4859(12)	11.9388(6)
c, Å	16.5863(11)	37.699(2)
β, deg	106.129(1)	93.165(2)
V, Å^3	3171.8(4)	3173.9(3)
Z	4	4
ρ_{calcd}, g cm^{-3}	1.213	1.212
μ, mm^{-1}	0.99	0.99
no. reflns measd.	19862	22094
no. unique reflns, R_{int}	5970, 0.028	5587, 0.041
no. reflns with $F^2 > 2\sigma(F^2)$	5733	4872
trans coeff range	0.790−0.866	0.827−0.908
R, R_w[a] ($F^2 > 2\sigma$)	0.021, 0.054	0.049, 0.099
R, R_w[a] (all data)	0.022, 0.055	0.057, 0.103
S[a]	1.041	1.196
refined params	296	296
max, min diff map, e Å^{-3}	0.37, −0.52	1.42, −1.37

[a] Conventional $R = \sum||F_o| - |F_c||/\sum|F_o|$; $R_w = [\sum w(F_o^2 - F_c^2)^2/\sum w(F_o^2)^2]^{1/2}$; $S = [\sum w(F_o^2 - F_c^2)^2/(\text{no. data} - \text{no. params})]^{1/2}$ for all data.

Crystal Structure Determinations of *rac*- and *meso*-6. For *rac*-**6**, measurements were made at 120 K on a Bruker Nonius APEX2 CCD diffractometer using a synchrotron X-ray source (λ = 0.6898 Å); for *meso*-**6**, measurements were made at 150 K on a Bruker AXS SMART CCD diffractometer using graphite-monochromated Mo Kα radiation (λ = 0.71073 Å). For both compounds, cell parameters were refined from the observed positions of all strong reflections in each data set. Intensities were corrected semi-empirically for absorption on the basis of symmetry-equivalent and repeated reflections. The structures were solved by direct methods and refined on F^2 values for all unique data. Table 2 gives further details. The hydrogen atoms of the BH_3 groups were located in difference maps and were freely refined. Non-hydrogen atoms were refined anisotropically, and all remaining H atoms were constrained with a riding model; U(H) was set at 1.2 (1.5 for methyl groups) times U_{eq} for the parent atom. Programs were Bruker AXS SMART (control) and SAINT (integration), and SHELXTL for structure solution, refinement, and molecular graphics.[23]

DFT Calculations. Geometry optimizations on the gas-phase molecules were performed with the Gaussian03 suite of programs (revision C.01)[24] on a cluster of Compaq ES40 Alphaservers, via the EPSRC National Service for Computational Chemistry Software (http://www.nsccs.ac.uk). Optimizations were performed using the B3LYP hybrid functional[18] with an Lanl2dz effective core potential basis set[19] for Sn and a 6-31G(d,p) all-electron basis set on the remaining atoms[20] (default parameters were used throughout). Minima were confirmed by the absence of imaginary vibrational frequencies. NBO analyses were performed using the NBO 3.0 module of Gaussian03.[22]

Acknowledgment. The authors are grateful to the Royal Society and the EPSRC for support and to the EPSRC-funded National Crystallography Service and CCLRC for access to synchrotron facilities. We thank Dr. C. Dennison and Dr. K. Sato for undertaking the EPR spectroscopy.

(23) (a) *APEX2, SMART and SAINT software for CCD diffractometers*; Bruker AXS, Inc.: Madison, WI, 2004 and 1997. (b) Sheldrick, G. M. *SHELXTL user manual*, version 6; Bruker AXS, Inc.: Madison, WI, 2001.

(24) Frisch, M. J. et al. *Gaussian 03*, rev C.01; Gaussian, Inc.: Wallingford CT, 2004.

Supporting Information Available: For *rac*- and *meso*-**6**, details of structure determination, atomic coordinates, bond lengths and angles, and displacement parameters in CIF format. For *rac*- and *meso*-**6a**, details of DFT calculations, final atomic coordinates, and energies. Complete details of ref 24. This material is available free of charge via the Internet at http://pubs.acs.org. Observed and calculated structure factor details are available from the authors upon request.

OM0600036